SUPPLEMENTARY INFORMATION
https://doi.org/10.1038/s41566-018-0144-1

nature photonics

In the format provided by the authors and unedited.

Mid-infrared frequency comb via coherent dispersive wave generation in silicon nitride nanophotonic waveguides

Hairun Guo[1,5], Clemens Herkommer[1,2,5], Adrien Billat[3,5], Davide Grassani[3], Chuankun Zhang[1,4], Martin H. P. Pfeiffer[1], Wenle Weng[1], Camille-Sophie Brès[3]* and Tobias J. Kippenberg[1]*

[1]Laboratory of Photonics and Quantum Measurements (LPQM), École Polytechnique Fédérale de Lausanne (EPFL), Lausanne, Switzerland. [2]Physik-Department, Technische Universität München (TUM), München, Germany. [3]Photonic Systems Laboratory (PHOSL), École Polytechnique Fédérale de Lausanne (EPFL), Lausanne, Switzerland. [4]Tsinghua University, Beijing, China. [5]These authors contributed equally: Hairun Guo, Clemens Herkommer, Adrien Billat. *e-mail: camille.bres@epfl.ch; tobias.kippenberg@epfl.ch

Supplementary Information: Mid-infrared frequency comb via coherent dispersive wave generation in silicon nitride nano-photonic waveguides

Hairun Guo[1,*], Clemens Herkommer[1,2,*], Adrien Billat[3,*], Davide Grassani[3], Chuankun Zhang[1,4], Martin H. P. Pfeiffer[1], Wenle Weng[1], Camille-Sophie Brès[3,†], Tobias J. Kippenberg[1,‡]

[1]*Laboratory of Photonics and Quantum Measurements (LPQM), École Polytechnique Fédérale de Lausanne (EPFL), CH-1015 Lausanne, Switzerland*

[2]*Physik-Department, Technische Universität München (TUM), D-80333 München, Germany*

[3]*Photonics Systems Laboratory (PHOSL), École Polytechnique Fédérale de Lausanne (EPFL), CH-1015 Lausanne, Switzerland*

[4]*Tsinghua University, Beijing 100084, China*

† *camille.bres@epfl.ch*

‡ *tobias.kippenberg@epfl.ch*

* *These authors contributed equally to the work.*

1 Large-size Si_3N_4 waveguides beyond cracking limitation.

The fabrication of large-size Si_3N_4 waveguides is challenging as the tensile stress in Si_3N_4 films by LPCVD can lead to cracks when the film thickness is increased. In practice, the maximum crack-free Si_3N_4 film thickness for our process was found to be $\sim 1.0\ \mu m$. Here we achieve the fabrication of a large-size Si_3N_4 waveguides with a height as large as $2.3\ \mu m$ using the photonic Damascene process [1]. Importantly, we make use of the high surface mobility provided by the dichlorosilane (SiH_2Cl_2) and ammonia (NH_3) chemistry during LPCVD. This allows a high conformality when depositing Si_3N_4 onto the pre-structured substrate. The result is shown in Fig. S1 on cross sections of filled trenches with different widths. In the panels (a) and (b), the cross sections were imaged after the planarization step, included in the photonic Damascene process flow. The dashed white line indicates the cross section of the Si_3N_4 film right after deposition. From Fig. S1 (b) it can be seen that the SiO_2 preform (blue) is conformally filled with Si_3N_4 (red), i.e. deposition rates for the film growing from the bottom and from the sides are similar. As the trench width approaches less than 2-times the film thickness (i.e. $2 \times 1.0\ \mu$m), the gap begins to close, as shown in Fig. S1 (a). This enables us to fabricate waveguides with a height of $2.3\ \mu$m and a maximum width of $1.8\ \mu$m. No voids were observed in such large-size waveguides. There is a slightly slanted sidewall angle of $\sim 85°$. An example of such a waveguide with a width of $1.6\ \mu$m is shown in Fig. 1 (c).

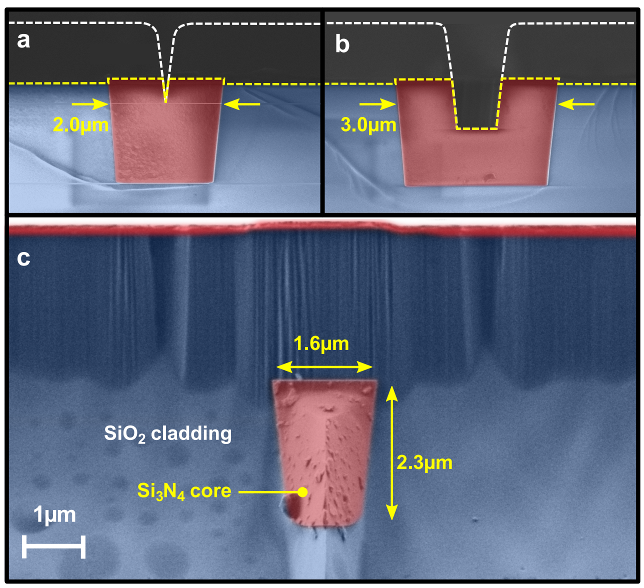

Figure S1: Cross sections showing the thick waveguide fabrication scheme. (a) and (b) show cross sections imaged with SEM after the surface planarization. The dashed white line indicates the cross section after Si_3N_4 deposition. From (b) it can be seen that the gap is filled conformally during the deposition, i.e. the film is growing at the same rate from the bottom as well as from the sides of the trench. The transition to a completely filled gap is shown in (a), as the trench width is reduced to ≤ 2 times the Si_3N_4 film thickness. A fabricated waveguide with a height of $2.3\ \mu$m and a width of $1.6\ \mu$m is shown in (c).

2 Mid-IR efficiency and spectral coverage.

Here we estimate the efficiency of mid-IR dispersive wave generation in the large-cross-section waveguides, which is done by NLSE-based simulations. For each simulated supercontinuum, the mid-IR wave packet is numerically "filtered" out and its power is compared to that of the full spectrum, calculated as the conversion efficiency. Moreover, the bandwidth of the mid-IR wave is also read out, cut at the -30 dB level compared to the peak. The estimation is then concluded as a figure of merit shown in Fig. S2.

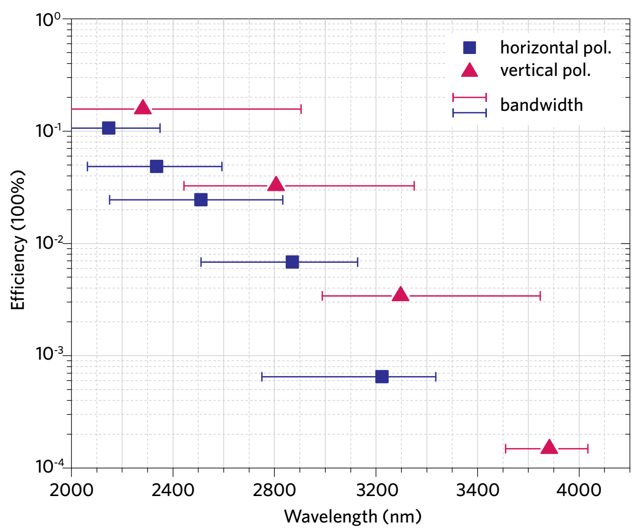

Figure S2: Figure of merit of mid-IR dispersive wave generation in large-cross-section waveguides. "Triangle" and "square" Symbols indicate the conversion efficiency as a function of the peak wavelength of the mid-IR wave packet. The conversion efficiency is calculated as the power of the mid-IR wave packet that is numerically "filtered" out and compared to the full spectral power. The scale bars indicate the bandwidth of the mid-IR wave, cut at the -30 dB level with respect to its peak. The rose-colored data corresponds to a vertically polarized pump source, while the blue-colored data is to the horizontally polarized pump. Among data points are different waveguide geometries, namely the width varying from 950 nm to 1100 nm.

Clearly, it can be observed that the conversion efficiency of the mid-IR wave is degraded when the generation is at longer wavelengths. The reason is that, in SPM-induced spectral broadening, the optical power is exponentially decaying in the sideband, leading to a reduced power fraction that is eventually coupled to form the dispersive wave when having the phase matching.

In experiments, while the wavelength coverage of mid-IR dispersive waves has been demonstrated (cf. Fig. 3(b) in the manuscript) and mostly matches with simulations, the efficiency is lower if compared to other approaches such as DFG. Also, there are a few loss issues including: the insertion loss, loss on the aspherical lens (-1.5 dB) for collecting the mid-IR wave, and possible scattering loss in waveguides as fabrication defects. These lead to the absolute power in the mid-IR to be below the milliwatt level at the moment. Ideally, with superior dispersion engineering, a conversion efficiency of $> 1\%$ can be obtained within the targeted mid-IR region ($2.5 - 4$ μm). Moreover, increasing the pump power can directly raise the power in the mid-IR. In particular, the increase of the average pump power to 1 Watt should be reasonably straightforward without compromising the complexity of the system in term of compactness and ease. To illustrate this point we mention, for example, the NKT Koheras Boostik module (used for LIDAR and wind sensing) with compact Erbium-fiber amplifiers that readily achieve 1 Watt output power though in CW mode. These options can be considered as alternatives to the current source in order to increase the power in the mid-IR to be tens of milliwatt.

3 Intensity and phase noise measurements.

Here we analyze the coherence of the supercontinuum (cf. Fig. 4(b) for the spectrum) in terms of the relative intensity noise (RIN) and the phase noise. Figure S3 shows the RIN of the generated supercontinuum compared to the pump source. In this measurement, the supercontinuum output is collected by a standard single-mode lensed fiber (spot diameter ~ 2.5 μm), meaning that most of the near-IR portion of the spectrum is transmitted but the mid-IR wave is attenuated. The measured power is ~ 2.2 mW. When measuring the intensity noise of the pump source, the pump power is attenuated to be matched to ~ 2.5 mW. The detector (Thorlabs, DET01CFC) has a spectral responsivity in the range $0.8 - 1.7$ μm, and a direct current (DC) saturation power of 5.5 μW.

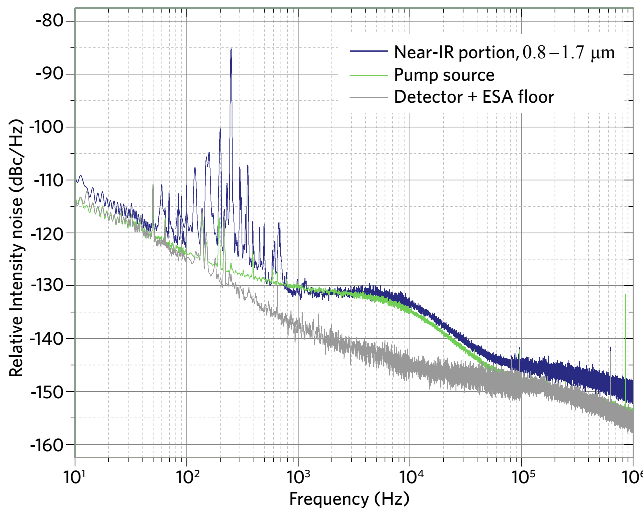

Figure S3: Relative intensity noise (RIN) of supercontinuum generation in the near-IR region. The green-colored trace indicates the RIN of the pump source (optical power adjusted to be $\sim 2.5\ \mathrm{mW}$). The blue-colored trace indicates the RIN of the near-IR portion of the generated supercontinuum (collected by a standard single-mode fiber based lensed fiber, measured power $\sim 2.2\ \mathrm{mW}$, detector responsivity range $0.8 - 1.7\ \mu\mathrm{m}$). Spikes found within the frequency range $50\ \mathrm{Hz} - 1\ \mathrm{kHz}$ are acoustic pick-ups mostly resulting from the lensed fiber coupling that is sensitive to vibrations. The gray-colored trace indicates the noise floor of the detector.

The RIN of the pump source and the near-IR supercontinuum is directly compared. It can be observed that the intensity noise trace of the supercontinuum follows that of the pump source in the frequency region $1 - 100\ \mathrm{kHz}$, while at lower frequency region, $50\ \mathrm{Hz} - 1\ \mathrm{kHz}$, strong acoustic pick-ups are introduced in the supercontinuum mostly due to the lensed fiber coupling that is sensitive to vibrations. Apart from that, no clear evidence is found that the supercontinuum process would raise the intensity noise.

The RIN of the mid-IR wave could unfortunately not be assessed since our mid-IR detector is not DC-coupled. In return, we measured the phase noise of the repetition-rate beat to assess the coherence of the mid-IR wave. Figure S4 shows the repetition rate phase noise of the mid-IR wave (filtered out by the edge-filter), which is compared to the near-IR portion of the supercontinuum as well as to the pump source. Note that the pump source has both the carrier-envelope offset and the repetition rate free running, which prevented us from measuring the phase noise below the frequency offset of $3\ \mathrm{Hz}$. The mid-IR wave is detected by an HgCdTe-based photovoltaic detector (Vigo PVI-4TE-10.6, integrated trans-impedance amplifier, bandwidth $10\ \mathrm{kHz} - 1\ \mathrm{GHz}$). The measurement was performed with an electronic spectrum analyzer (Rohde & Schwarz, FSW series).

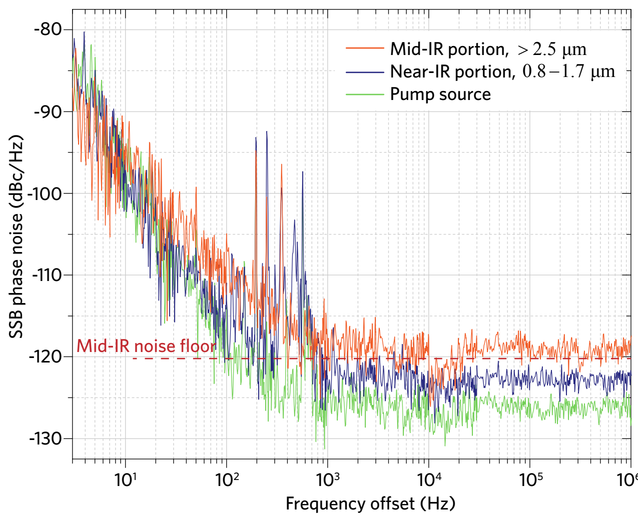

Figure S4: Single sideband phase noise of supercontinuum generation in both mid-IR and near-IR. The phase noise is with respect to the repetition rate beatnote ($100\ \mathrm{MHz}$) of the pump laser as well as the near- and mid-IR portion of the supercontinuum. The green-trace indicates the phase noise of the pump source. The blue-trace indicates the phase noise of the near-IR portion of the generated supercontinuum ($0.8 - 1.7\ \mu\mathrm{m}$). The orange-colored trace indicates the phase noise of the mid-IR portion of the generated supercontinuum that is filtered out in free space by the edge-filter cut on at $2.5\ \mu\mathrm{m}$. The electronic power of the repetition single is $-29.11\ \mathrm{dBm}$ for the pump, $-26.70\ \mathrm{dBm}$ for the near-IR portion, and $-21.27\ \mathrm{dBm}$ for the mid-IR portion.

As a result, it was observed that the phase noise of the pump, the near-IR continuum and the mid-IR wave overall match with each other, meaning that the mid-IR wave maintains a good level of coherence through the supercontinuum process. In detail, the slope of the noise in the pump as well as in the near-IR continuum is on the level of $-20\ \mathrm{dB/decade}$, reflecting the white frequency fluctuation of a free-running laser oscillator, while the mid-IR portion shows a higher noise level in the range $30\ \mathrm{Hz} - 1\ \mathrm{kHz}$ with a slope of $-10\ \mathrm{dB/decade}$ indicating the emergence of flicker phase fluctuation. Beyond $1\ \mathrm{kHz}$, the phase noise of the mid-IR wave reaches the noise floor of $-120\ \mathrm{dBc/Hz}$.

References

1. Pfeiffer, M. H. P. *et al.* Photonic damascene process for integrated high-Q microresonator based nonlinear photonics. *Optica* **3**, 20–25 (2016).